Disorder-to-order transition of the amyloid-β peptide upon lipid binding

Hebah Fatafta[1,#], Batuhan Kav[1,#], Bastian F. Bundschuh[2], Jennifer Loschwitz[1,2], Birgit Strodel[1,2,*]

[1] *Institute of Biological Information Processing (IBI-7: Structural Biochemistry), Forschungszentrum Jülich, 52425 Jülich, Germany*

[2] *Institute of Theoretical and Computational Chemistry, Heinrich Heine University Düsseldorf, Universitätstrasse 1, 40225Düsseldorf, Germany*

[*] *Corresponding author: b.strodel@fz-juelich.de*
[#] *These authors contributed equally.*

Abstract

There is mounting evidence that Alzheimer's disease progression and severity are linked to neuronal membrane damage caused by aggregates of the amyloid-β (Aβ) peptide. However, the detailed mechanism behind the membrane damage is not well understood yet. Recently, the lipid-chaperone hypothesis has been put forward, based on which the formation of complexes between Aβ and free lipids enables an easy insertion of Aβ into membranes. In order to test this hypothesis, we performed numerous all-atom molecular dynamics simulations. We studied the complex formation between individual lipids, considering both POPC and DPPC, and Aβ and examined whether the resulting complexes would be able to insert into lipid membranes. Complex formation at a one-to-one ratio was readily observed, yet with minimal effects on Aβ's characteristics. Most importantly, the peptide remains largely disordered in 1:1 complexes, and the complex does not insert into the membrane; instead, it is adsorbed to the membrane surface. The results change considerably once Aβ forms a complex with a POPC cluster composed of three lipid molecules. The hydrophobic interactions between Aβ and the lipid tails cause the peptide to fold into either a helical or a β-sheet structure. These observations provide atomic insight into the disorder-to-order transition that is needed for membrane insertion or amyloid aggregation to proceed.

1. Introduction

Intrinsically disordered proteins (IDPs) are a family of proteins that are generally characterized by lacking a well defined structure. Instead, they are disordered and can adopt a variety of conformations in their physiological environment [1, 2]. Interestingly, this disordered nature is essential for IDPs in order to perform diverse biological functions, such as regulation in cell cycling, transcription, and translation [3, 4, 5, 6]. Several, if not most, IDPs undergo a function-related disorder-to-order transitions upon binding to a specific interaction partner, allowing them to mediate multiple interactions with different partners in the cell [7, 8, 9, 10, 11, 12]. A recent review discussed how such disorder-to-order transitions can be characterized using molecular dynamics (MD) simulations [13]. When misexpressed, mismodified, misprocessed, and/or dysregulated, IDPs are connected to the development of various diseases [14], including amyloidosis [15], diabetes [16], and neurodegenerative diseases[17, 18] in humans. Notably, many of these diseases are associated with amyloid forming proteins, which are proteins that assemble into pathogenic, insoluble aggregates including oligomers, protofibrils, and fibrils [19].

One member of the IDP and amyloid-protein families that gained particular attention is the amyloid-β (Aβ) peptide, which is strongly linked to the development of Alzheimer's disease (AD) [20, 21]. Aβ is generated through the cleavage of the transmembrane amyloid precursor protein [22, 23]. It ranges from 39 to 43 amino acids in length, with Aβ_{42} being the predominant alloform in the amyloid fibrils that lead to senile plaques. Moreover, Aβ_{42} is also more toxic than Aβ_{40}, which is the most common alloform. Mounting evidence suggests that the toxicity related to Aβ is exerted via abnormal interactions of the Aβ aggregates with the neuronal cell membrane [24, 25]. The small-sized amyloid oligomers are found to be more toxic than the mature fibrils [26, 27, 28]. Unfortunately, the detailed molecular mechanism of the Aβ–membrane interaction is still not fully resolved. Therefore, further stud-

ies aiming to understand these interactions and the resulting membrane-damaging mechanisms are warranted and needed.

Numerous studies that explored Aβ–membrane interactions focused on Aβ in a water-membrane environment. They typically aimed to identify the key players, such as Aβ oligomers or fibrils, and the membrane-damage mechanisms, such as membrane pore formation or detergent-like membrane thinning [29, 30, 31]. Common to these studies is that they investigate the behavior of Aβ in a lipid-rich phase, i.e., in the presence of a lipid membrane. However, recent studies demonstrated the crucial role of free lipids, which exist at nanomolar to micromolar concentration in equilibrium with the membrane, in the formation of Aβ-lipid complexes, which enabled an easy membrane insertion for Aβ and also other amyloid proteins [32, 33]. Based on these results, La Rosa and coworkers proposed a lipid-chaperone hypothesis as a unifying framework for amyloid-membrane poration [34]. Some experimental and MD studies reported on the stability of peptide-lipid complexes in solution and their role in assisting protein transport into membranes [34, 32, 35]. In general, lipid-assisted protein transport is overlooked compared to the well documented lipid-carriage by proteins [36, 37, 38].

In this study, we perform all-atom MD simulations to investigate two aspects of the lipid-chaperone hypothesis: (i) complex formation between Aβ_{42} and lipid molecules in 1:1 and 1:3 ratios in solution, (ii) interaction of the Aβ_{42}–lipid complexes with pre-assembled lipid membranes. As lipids we chose the most abundant lipids in mammalian cells: 1-palmitoyl-2-oleoyl-sn-glycero-3-phosphocholine (POPC) and 1,2-dipalmitoyl-sn-glycero-3-phosphocholine (DPPC) (Fig. 1). We find that Aβ_{42} forms stable complexes with both lipid molecules. While the peptide remains largely disordered in the 1:1 complexes, it undergoes disordered-to-ordered transitions upon interaction with three lipid molecules. However, on the microsecond timescale of our simulation no membrane insertion is observed for the Aβ_{42}–lipid complexes, while a single lipid can readily integrate into an existing membrane on the same timescale.

2. Methods

2.1. System setup

We performed all-atom MD simulations for three Aβ_{42}–lipid systems: 1:1 complexes in solution, 1:3 complexes in solution, and 1:1 complexes in a membrane environment. For the systems involving 1:1 complexes, we performed two sets of simulations: a reference set and a target set, as described below and summarized in Table 1.

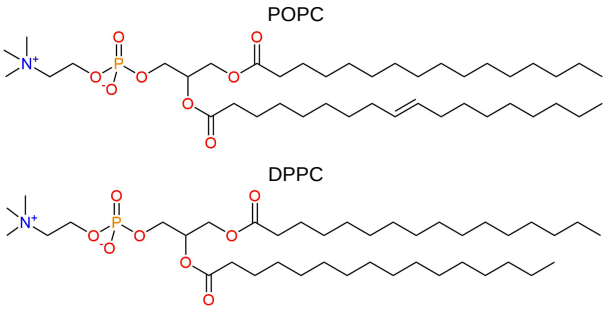

Figure 1: Chemical 2D–structure of 1-palmitoyl-2-oleoyl-sn-glycero-3-phophocholine (POPC, top) and 1-2-dipalmitoyl-sn-glycero-3-phosphocholine (DPPC, bottom).

Table 1: Summary of simulations performed in this work.

System	**Runs $\times$ length**
1 Aβ_{42}	$3 \times 1\ \mu$s
1:1 Aβ_{42}–DPPC	$3 \times 1\ \mu$s
1:1 Aβ_{42}–POPC	$3 \times 1\ \mu$s
1:3 Aβ_{42}–POPC	$3 \times 2\ \mu$s
1:1 Aβ_{42}–POPC + POPC membrane	$3 \times 2\ \mu$s
1 Aβ_{42} + POPC membrane	$1 \times 2\ \mu$s
1 POPC + POPC membrane	$1 \times 2\ \mu$s
Total simulation time	**25 μs**

1:1 Aβ_{42}–lipids complexes. We followed the complex formation between Aβ_{42} and a single lipid molecule, either POPC or DPPC, in solution by placing them in a simulation box with an initial minimal distance of 4 nm between them, which was realized with Packmol [39]. This setup defines the target state for the 1:1 complexes, while the reference is a single Aβ_{42} peptide in solution. As starting structure for Aβ_{42} a random-coil conformation was used. It was retrieved from a 30 μs MD simulation of Aβ_{40} that employed the Amber99SB-UCB force field [40, 41]. The two C-terminal residues Ile41 and Ala42 were added to obtain Aβ_{42}. Each simulation was run for 1 μs and in triplicate using different initial velocities. The total number of atoms in these systems was $N \approx 50,000$ and the simulation box volume V measured $8.0 \times 8.0 \times 8.0$ nm^3.

1:3 Aβ_{42}–POPC complexes. To study the behavior of Aβ_{42} in the presence of three POPC lipids, we identified the most populated conformation of the 1:1 Aβ_{42}–POPC

complex and added two more POPC lipids to it. The two additional POPC molecules were placed randomly using Packmol, with a minimum distance of 4 nm from the existing 1:1 complex and between each other. For this setup, 2 μs MD simulations were performed in triplicate with different initial velocities. The total number of atoms in these systems was $N \approx 50,000$ and the simulation box volume V measured $8.0 \times 8.0 \times 8.0$ nm^3.

1:1 Aβ_{42}–lipids complexes plus membrane. A lipid bilayer composed of 154 POPC lipids was generated using the CHARMM-GUI interface [42]. The reference set includes two setups: one involving a single Aβ_{42} peptide plus the membrane, the other one including a single POPC lipid plus the membrane. The target system is a 1:1 Aβ_{42}–POPC complex plus the membrane. The peptide, lipid or complex were placed at a minimal distance of 1.0 nm above the bilayer surface in the water layer. All systems were simulated for 2 μs, and in the case of the target system, the system was simulated in triplicate with different initial velocities. The total number of atoms in these systems was $N \approx 134,000$ atoms and and the simulation box volume measured $10.0 \times 10.0 \times 14.0$ nm^3.

2.2. Simulation details

The MD simulations were performed using GROMACS version 2018 [43]. Aβ_{42} was modeled using the CHARMM36mW force field [44], as this force field provides acceptable results for the amyloid-β peptide [41] and was identified as the currently most suited force field for simulating amyloid aggregation [45]. The CHARMM36 force field [46] was applied to the lipids. All systems were solvated using the TIP3P water model [47, 48] and NaCl was added at a physiological concentration of 150 mM. Each system was first energy minimized using the steepest decent algorithm to remove atomic clashes. This was followed by equilibration MD simulations of 0.1 ns length and under NVT conditions where the temperature T was kept at 310 K using a velocity-rescaling thermostat [49]. Next, the systems were equilibrated for 1 ns under NpT conditions to obtain a pressure p of 1.0 bar. The pressure was regulated using the isotropic (for the simulations without a lipid membrane) or semi-isotropic (for the simulations involving a lipid membrane) Parrinello-Rahman pressure coupling scheme [50]. Periodic boundary conditions were applied in all directions and the particle mesh Ewald method [51] was used for calculating the electrostatic interactions. Both the short-range Coulomb interactions and the van der Waals interactions were cut at 1.2 nm in real space.

2.3. Analysis

The analysis of the simulations was performed using a combination of GROMACS tools and the MDTraj library. We calculated the root mean square fluctuations (RMSF) of the Aβ_{42} residues using the GROMACS tool *rmsf*. The secondary structure of the peptide was determined using the DSSP algorithm [52] and time-averages calculated, which are provided as secondary structure propensities. Here, we collectively present α-, π- and 3_{10}-helices as helical propensity, β-bridges are included in the β-strand propensities, and bends and β-turns are collectively shown as turn propensities. The solvent accessible surface area (SASA) of Aβ_{42} was determined using the GROMACS tool *sasa*. We calculated the number of contacts between $A\beta_{42}$ and the lipids, which either form a complex with the peptide or are part of the membrane, using a 0.5 nm distance cutoff between the protein backbone atoms and the lipid atoms (excluding lipid hydrogen atoms). We provide contact probabilities, which are the ratio between the number of MD snapshots with Aβ_{42}–lipid contacts being present and the number of snapshots in the corresponding MD trajectory.

3. Results

3.1. Complex formation between Aβ_{42} and soluble lipids

3.1.1. 1:1 Aβ_{42}–lipid complexes

We investigate the interactions between Aβ_{42} and single POPC or DPPC lipids using unbiased all-atom MD simulations using three distinct systems: a single Aβ_{42} peptide in solution, a single Aβ_{42} peptide with one soluble POPC lipid, and a single Aβ_{42} peptide with one soluble DPPC lipid. For each system, we run three independent simulations, each of which was 1 μs long. The single Aβ_{42} peptide serves as a reference, to unravel the effects of a POPC or DPPC lipid on the structure of Aβ_{42}.

The formation of Aβ_{42}–lipid complexes reduces the peptide flexibility. In all of our simulations involving both a Aβ_{42} peptide and a lipid molecule, a stable protein-lipid complex formed within the first 100 ns and did not dissociate in the rest of the simulations (Fig. S1). This indicates that the lifetimes of these complexes is longer than microseconds. Representative complex snapshots are shown in Fig. 2a and b. To investigate how the complex formation affects the peptide flexibility, we calculated the RMSF of each peptide residue after the Aβ_{42}–lipid complex had formed, and compare

these results to the case of a single Aβ_{42} in solution (Fig. 2c). For most residues we observe a reduction in the RMSF upon complex formation. The increase in peptide rigidity is especially pronounced for the hydrophobic regions of Aβ_{42}, which are the central hydrophobic core involving residues Leu17–Ala21 and the C-terminal residues Ala30–Ala42. The formation of Aβ_{42}–DPPC complexes imposes more rigidity on Aβ_{42} than complexation with POPC, particularly in the region Asp1–Val24. Furthermore, the calculation of the SASA indicates that the complex formation reduces the peptide's accessibility to the solvent. The SASA values of Aβ_{42} are 45.7 ± 1.3, 43.9 ± 1.2 and 40.6 ± 1.2 nm^2 for an individual Aβ_{42} peptide, for Aβ_{42} in complex with a POPC molecule and in complex with a DPPC molecule, respectively. The larger reductions in peptide flexibility and SASA in the case of DPPC as compared to POPC suggest that the interactions between Aβ_{42} and DPPC are stronger and/or involve more Aβ_{42} residues.

Small increase in β-sheet but no helix upon 1:1 complex formation. To characterize the effect of the complex formation on the peptide secondary structure, we calculated both the evolution of the secondary structure per residue (Fig. S2) and the time-averaged secondary structure for the whole peptide (Fig. 2d) and compare the results to the findings for the individual Aβ_{42} peptide. The time-averaged data reveal an increase in turn structures upon complex formation with either lipid. Furthermore, the binding to DPPC, but not POPC, encouraged more β-strands to be formed, which happened at the expense of random coil structures. Aβ_{42} shows a very small propensity for helix formation, which almost completey disappears following binding to DPPC. Only the time-evolution plots of the secondary structure shown for each MD simulation (Fig. S2) reveals that also in the presence of DPPC some helical structures existed, yet only for short amounts of time. These plots further disclose that the β-strands that formed in the case of the Aβ_{42}–DPPC complexes are part of a β-sheet that was established in the N-terminal half of the peptide, mainly involving residues Ser8–Phe20 with a turn at His13/His14. This β-sheet was established in all three simulations involving DPPC and in one of the simulations with POPC. However, it was not present in the other two Aβ_{42}–POPC simulations and also not in the simulations of the isolated Aβ_{42} peptide. In the latter, some helix formation is observed in the N-terminal region of Aβ_{42}, which disappears upon complex formation with either lipid. In summary, while the time-averaged secondary structure does not indicate large effects on the Aβ_{42} structure, the detailed analysis does show that the Aβ_{42}–lipid interactions change the peptide's structural preferences.

The lipid tails dominate the interaction with Aβ42. To elucidate the dominant peptide–lipid interactions, we calculated the contacts between Aβ_{42} residues and the POPC or DPPC lipid. The results in Fig. 2e reflect that the tails of the lipid molecules contribute more to the the peptide–lipid contacts than the headgroups. Moreover, both lipid tails of either lipid are involved in contact formation with Aβ_{42}. In particular, the oleoyl and the palmitoyl chain of POPC contribute similarly in driving Aβ_{42}–POPC interactions. POPC interacts with many of the Aβ_{42} residues, yet with most of them with a rather low probability, whereas the interaction with DPPC is mainly established by a few but prevailing contacts. In either case, the region Glu22–Gly29, which contains several charged and polar residues and has a tendency to lead to a turn in Aβ conformations, has a very low tendency to interact with the lipids, neither with their headgroups nor the tails. Aβ_{42} binds POPC preferably through residues Ala2–Phe4, Gly9–Glu11, Leu17–Phe30, and Ile31–Val40, while the binding to DPPC is concentrated on Phe4, Gln15, Val18–Phe20, and Ala30–Ile32. Apart from Gln15, these are all hydrophobic residues, indicating that in the binding with DPPC hydrophobic interactions are more important than in the interaction with the monounsaturated POPC lipid. The Aβ_{42} regions involved in binding to POPC or DPPC are the same residues that exhibit a reduced flexibility.

3.1.2. 1:3 Aβ$_{42}$–lipids complexes

Since the single lipid molecules seem to have no pronounced effects on Aβ_{42}, we decided to test whether a few more lipids, which are still in solution and not part of a membrane, can induce structural changes in Aβ_{42}. To this end, we added two more POPC lipid molecules to the 1:1 Aβ_{42}–POPC lipid complex, using the most stable 1:1 complex encountered in our simulations as a starting point, and simulated this system three times 2 μs.

Complex formation with 3 POPC molecules triggers a disorder-to-order transition of Aβ$_{42}$. Similar as for the 1:1 systems, association between the existing 1:1 complex and the two additional POPC molecules is readily observed within the first 50 ns, as revealed by the evolution of the minimal distance between Aβ_{42} and the lipids (Fig. S3). These 1:3 complexes are stable and did not disintegrate in the remainder of the simulations. A major difference between the 1:1 and 1:3 complexes

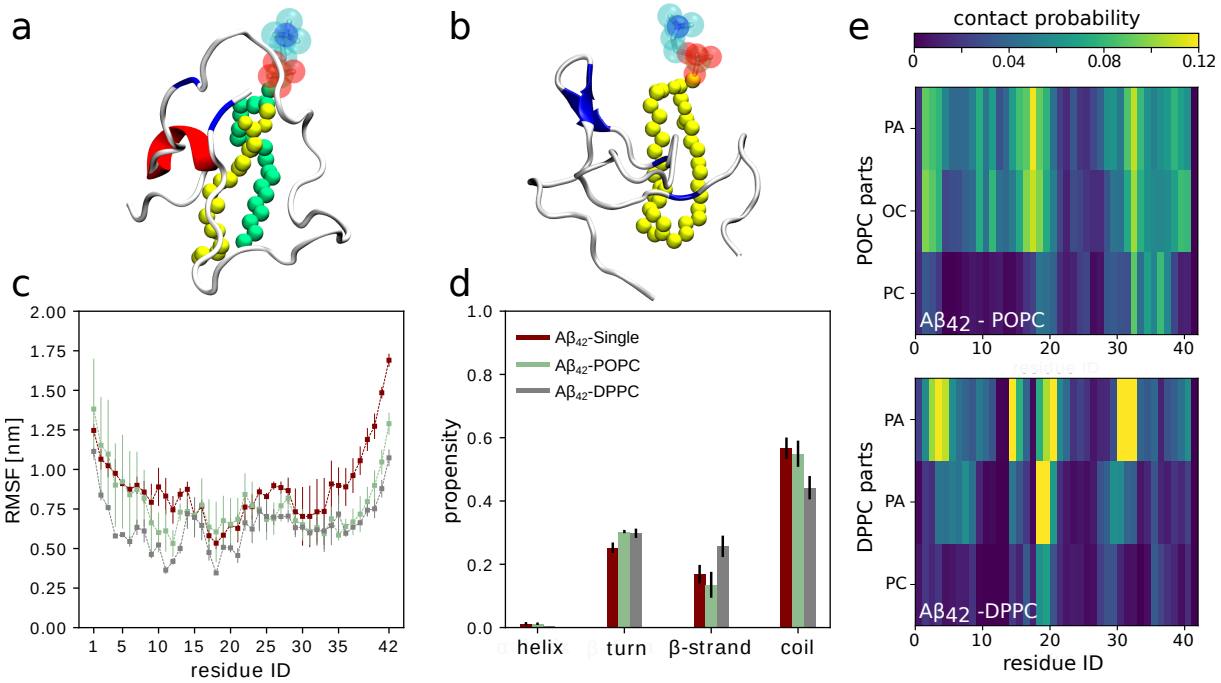

Figure 2: Summary of the results for the 1:1 Aβ_{42}–lipid complexes. (a) and (b) Snapshot of an Aβ_{42}–POPC and Aβ_{42}–DPPC 1:1 complex, respectively. Aβ_{42} is depicted as cartoon, with the helix being colored in red, *beta*-structures in blue, and the rest in white. POPC and DPPC are shown with spheres, using yellow for the palmitoyl chains, green for the oleoyl chain, red for the phosphadidyl group, and blue for the choline moiety. (c) The average RMSF and (d) the secondary structure propensities of Aβ_{42}, where being an individual peptide (red) or in complex with a POPC lipid (green) and DPPC (gray). The values are averaged over three independent runs and error bars represent the standard error of the mean. (e) The average contact probabilities between the Aβ_{42} residues and POPC (top) and DPPC (bottom) in the 1:1 complexes. The lipids are divided into their phosphocholine headgroups (PC) and their tails: the oleoyl (OL) and palmitoyl (PA) chains of POPC and two PA chains in DPPC. The contact probabilities are color-coded according to the color bar at the top.

is that in the latter Aβ_{42} underwent a random coil-to-helix transition (in MD run 1) or a random coil-to-β-sheet transition (in MD runs 2 and 3), as the evolution of these structural elements in Fig. 3a shows. In run 1 we observe a high α-helix content, where about 45% of the Aβ_{42} residues adopt a helical conformation after ≈800 ns of simulation time. Inspection of the helical conformation that formed reveals that it is a helix-kink-helix structure (Fig. 3b), which was stable in the last 200 ns of the simulation. In the other two runs, transient helix formation was observed too, especially in the first 500 ns of run 2, yet in the end the dominating secondary structure were β-sheets. In both run 2 and run 3, at certain times more than 30% of the Aβ_{42} residues are part of a β-sheet. The corresponding structures are shown in Fig. 3b. We can thus conclude that, when Aβ_{42} is surrounded by a sufficient number of lipids, it undergoes a disorder-to-order transition. This is a characteristic of IDPs, which commonly adopt more ordered states upon binding with their targets, which is also known as a coupled binding-and-folding process.

Hydrophobic Aβ_{42}–lipid interactions drive the binding-and-folding process. In order to understand the driving force behind the folding of Aβ_{42} into the helix-kink-helix structure, we calculated the number of contacts formed between the peptide and POPC lipids. The number of these contacts is correlated with the α-helical content (Fig. 3c). For run 1 one can clearly see that the more residues adopt a helical structure, the more contacts between Aβ_{42} and the lipids exist. However, a large number of Aβ_{42}-POPC contacts is not a guarantee for an α-helix to be formed, as for the other two runs, where the helical content did not increase beyond 20%, a similar amount of peptide-lipid contacts were formed. We thus reason that the α-helix content is likely to be correlated with specific residue-POPC contacts, rather than the total number of contacts. In order to test this idea, we calculated the correlation coefficient between the α-helix content and the Aβ_{42} residue-POPC contacts, considering residue singlets, duplets, triplets etc. We increased the number of residue groups until the correlation coefficient did not further improve. For run 1 we find that the contacts between POPC lipids and residues Leu17, Ala21, Ile32, and Val36 have a correlation coefficient of 0.8 with the α-helix content. For run 2, this contact-helix correlation is the highest for the residue pair Leu17 and Ser26, reaching a value of 0.5. Only for run 3, we did not observe any significant correlation (all coefficients < 0.2).

When inspecting the residue-resolved secondary structure evolution, one observes that all the POPC-contacting residues leading to a high correlation coefficient are also part of a helix. This is also highlighted in the representative helix-kink-helix structure that is shown in Fig. 3b. One can see that the helical conformation is stabilized by hydrophobic interactions between the lipid tails and Leu17 and Ala21 of the first helix as well as Ile32 and Val36 of the second helix. To verify this observation, we plotted the evolution of the number of atom-atom contacts formed between POPC and Leu17, Ala21, Ile32, and Val36 along with the evolution of the α-helix content (Fig. 3a). Indeed, from this kind of plot for run 1 we notice that the helical structure is only stable when the mentioned residues are simultaneously in contact with the lipids. In run 2, the amount of these contacts initially rises, leading to a transient increase in the helical content, yet at ≈500 ns both the number of these contacts and the helical content drop. Instead, β-sheet structures developed in runs 2 and 3, for which representative structures are shown in Fig. 3b. One can see that β-sheets can develop in different parts of the peptide: between N-terminal and C-terminal residues in run 2 and between hydrophobic stretches that include residues Leu17, Ala21, Ile32, and Val36 in run 3. A difference between the helix-kink-helix structure from run 1 and these two β-sheet structures is that in the latter the three lipids adopted an orientation as in a bilayer, with two of the lipids start forming one leaflet and the third lipid would be part of the opposite leaflet. In run 1, on the other hand, the three lipids rather interact with Aβ_{42} than with themselves. This observation suggests that Aβ_{42}-lipid interactions in solution can encourage α-helix formation, which might in turn cause Aβ_{42} to enter the lipid membrane, as proposed by the lipid-chaperone hypothesis [34], and once fully inserted into the membrane, it converts into β-sheets with the strands being parallel to the lipid tails, as can be seen in Fig. 3b.

3.2. Interaction between the complexes and a lipid bilayer

To examine if the Aβ_{42}–lipid complexes can indeed enhance the peptide insertion into a lipid membrane, we simulated the most stable Aβ_{42}–POPC lipid complex from the preceding 1:1 complex simulations in the presence of a POPC bilayer. For comparison, we also simulated a single Aβ_{42} peptide and a single POPC lipid placed above a POPC membrane. For the latter, i.e., the reference systems, we performed one 2 μs MD simulation each, while for the target system we run three independent 2 μs MD simulations.

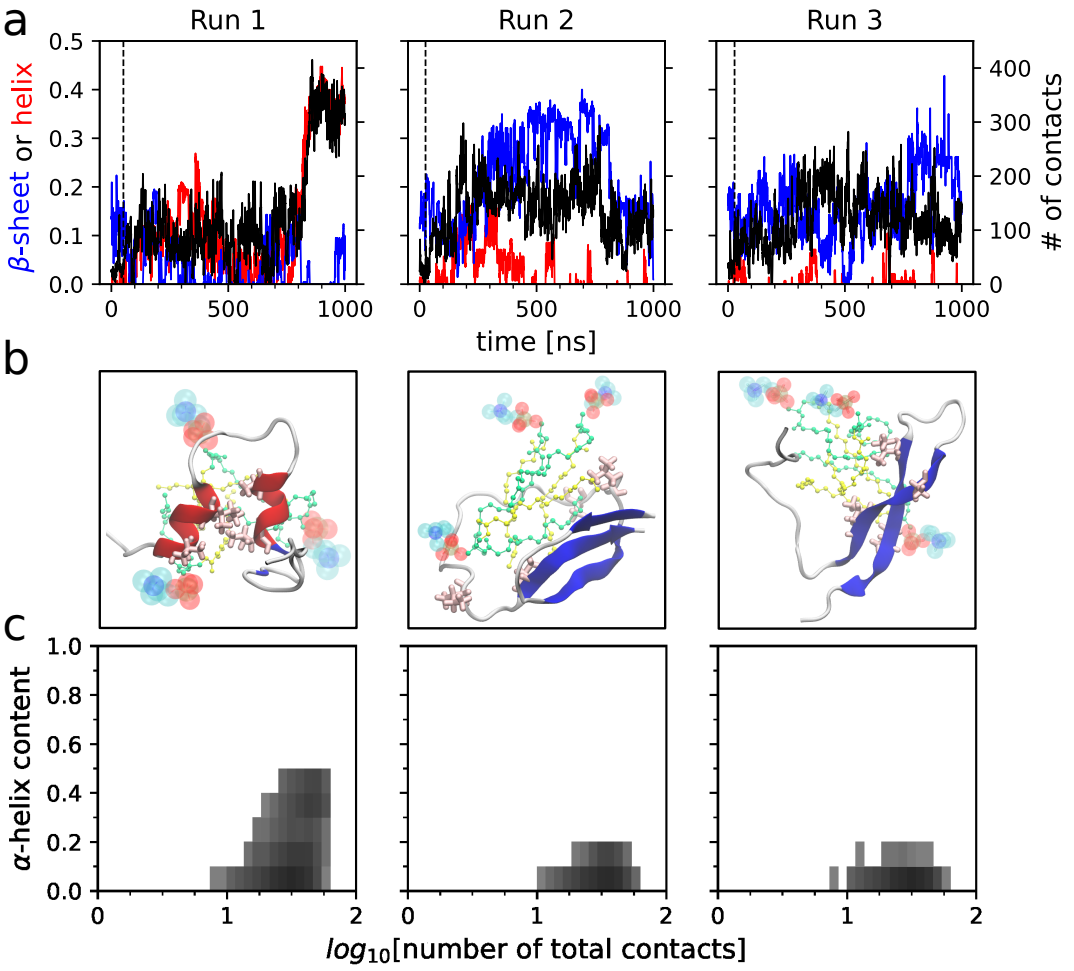

Figure 3: Summary of the results for the 1:3 Aβ_{42}–POPC complexes. (a) Evolution of the β-sheet (blue) and helix content (red) as well as the number of atom-atom contacts formed between the POPC lipids and Aβ_{42} residues Leu17, Ala21, Ile32, and Val36 obtained from the three simulations of 1:3 Aβ_{42}–POPC complexes. The dashed vertical lines mark time when all three POPC lipids had bound to Aβ_{42}. (b) Representative snapshots showing the helix-kink-helix structure that formed at the end of run 1 and β-sheet structures sampled in runs 2 and 3. The peptide is shown as cartoon and the sidechains of Leu17, Ala21, Ile32, and Val36 are explicitly shown. The lipid headgroups are indicated by blue and red spheres, and the oleoyl and palmitoyl chains are represented as ball-and-stick model in green and yellow color, respectively. (c) Two-dimensional histograms of the number of Aβ_{42}–POPC contacts plotted against the α-helix content. The darker the color of a bin, the more likely this contact-helix combination is.

A POPC lipid inserts into the membrane but not Aβ_{42}. Upon visualizing the trajectories we observed that all simulated entities, i.e., Aβ_{42}, a single POPC lipid, and the Aβ_{42}–POPC complex interacted with the lipid bilayer (Fig. S4). After a few attempts, the single POPC lipid even fully inserted into the lipid bilayer after 950 ns of simulation time. We show the intermediate steps occurring during the insertion process in Fig. 4. At t = 940 ns, the first contact between the lipid and the membrane, which eventually leads to successful insertion, is established via the palmitoyl chain. This causes the lipid to rotate by ≈90°, aligning it parallel to the membrane surface. Only one nanosecond later, the oleoyl chain has inserted into the headgroup region, making contact with the hydrophobic membrane core. The palmitoyl chain follows suit and also starts inserting into the membrane at t = 945 ns. This encourages the full insertion of the POPC lipid into the membrane, which is completed at t = 950 ns. Thus, the insertion process itself lasted only 10 ns. Together with the fact, that this event was recorded within a microsecond of simulation time, this indicates that such insertion processes can take place on a (sub)microsecond timescale if a molecule has a high driving force to enter into a membrane. In other words, if Aβ_{42}, alone or in complex with a lipid, should have a low free energy barrier

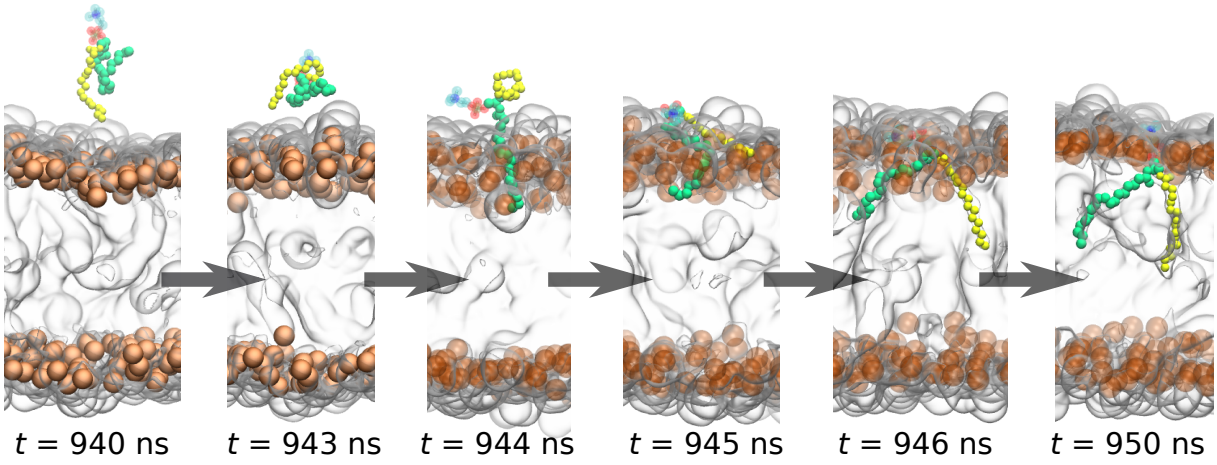

Figure 4: Snapshots of a POPC molecule inserting into a POPC membrane. At t = 940 ns the first contact between the POPC lipid and membrane was established and at t = 950 ns the insertion was completed. The oleoyl and palmitoly chains of the inserting lipid are shown in green and yellow, respectively. The POPC membrane is shown as translucent surface, with the lipid phosphate groups being indicated by orange spheres.

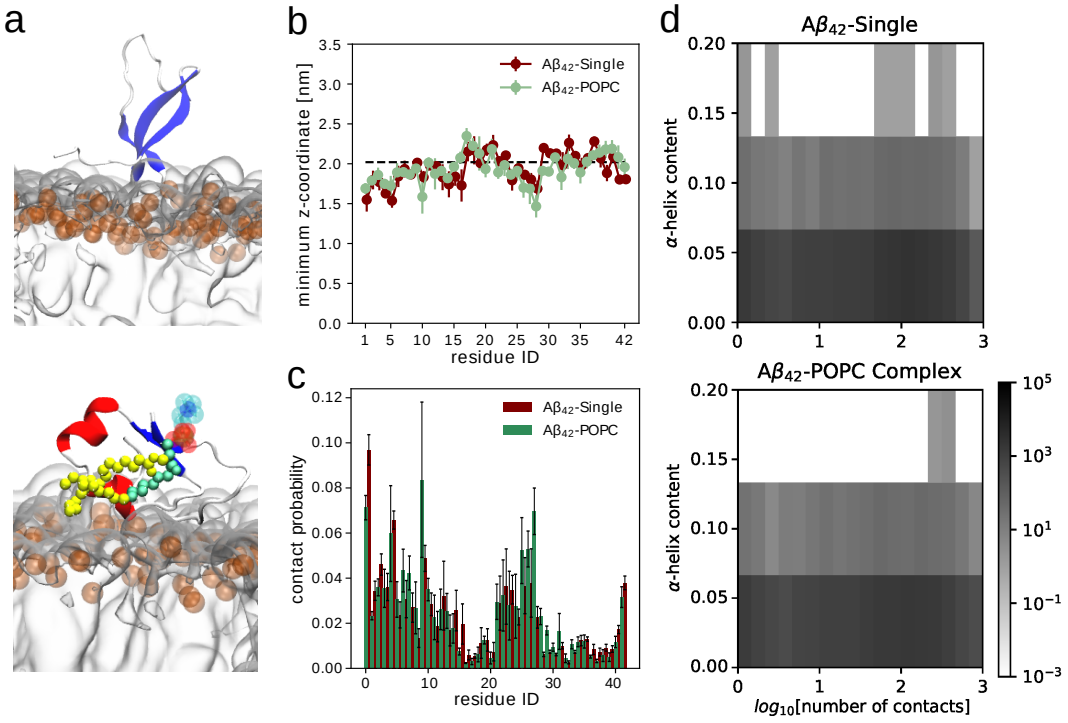

Figure 5: Summary of the results for the membrane simulations. (a) Snapshots of Aβ_{42} interacting with the POPC membrane, either for the individual peptide (top) or as part of the Aβ_{42}–POPC lipid complex (bottom). The same representations for the peptide, lipid, and membrane as in the previous figures were applied. (b) The minimum z-coordinates of the peptide residues for Aβ_{42} alone (red) and when in complex with a POPC lipid (green). The horizontal dashed line indicates the membrane surface, which is calculated as the half of the distance between the lipid-headgroup density profile peaks. (c) The corresponding probabilities of contact formation between the Aβ_{42} residues and the POPC membrane. The values are averaged over three independent runs and error bars represent the standard error of the mean. (d) Two-dimensional histograms of the number of Aβ_{42}–membrane contacts plotted against the α-helix content. The darker the color of a bin, the more likely this contact-helix combination is (number of occurrences according to the color bar).

to insert into a lipid membrane, we should be able to simulate this event by standard MD simulations.

However, the Aβ_{42} peptide did not insert into the membrane, also not when in complex with a POPC lipid. In these cases, only membrane adsorption is observed. Representative snapshots for these events are shown in Fig. 5a. That no membrane insertion occurred is evident from the average minimum z-coordinate (the bilayer normal is along the z-axis) of the peptide residues (Fig. 5b). We observe that parts of Aβ_{42} when in complex with POPC can insert more deeply into the membrane than the single Aβ_{42} peptide. This insertion is especially pronounced around residue Tyr10 and Gly25–Met35. These involve some of the residue regions that have significant contacts with the oleoyl and palmitoyl chains of the POPC lipid that is in complex with the peptide (Fig. 2e), which suggests that the single lipid is directly involved in the membrane insertion of Aβ_{42}. This assumption is further confirmed by the representative snapshot in Fig. 5a (bottom) that shows that the single POPC lipid mediates some of the Aβ_{42}–membrane contacts. Moreover, as Aβ_{42} has an overall charge of −3, it also screens the electrostatic repulsion between the peptide and the negatively charged phosphate groups of the POPC membrane, enabling a larger contact area between Aβ_{42} and the membrane to be formed. This can be deduced from the insertion depth in Fig. 5b and the representative snapshots in Fig. 5a for the membrane-adsorbed single peptide and the Aβ_{42}–lipid complex, respectively.

The average contacts occurring between Aβ_{42} and the lipid bilayer also reveal more initimate membrane interactions for the Aβ_{42} peptide when in complex with a POPC lipid (Fig. 5c). First of all, in this case Aβ_{42} forms more contacts with the lipid bilayer than an individual Aβ_{42} peptide. These differences are most pronounced in the regions Arg5–Gln15 and Gly25–Met35, which are the same residues that insert most deeply into the membrane in the case of the Aβ_{42}–POPC complex. By far the most contacts are formed by Tyr10, suggesting that this residue might play a key role in the membrane insertion of Aβ_{42}. Regarding the single Aβ_{42} peptide, residues Asp1–Arg5 and Gln15–Gly25 are the ones that form more contacts with the lipid bilayer than the other residues, also in comparison to the same residues in the 1:1 complex. These observations clearly demonstrate the different interaction patterns between Aβ_{42} and the POPC bilayer, depending on whether or not Aβ_{42} is in a bound complex with a lipid.

The Aβ_{42}–membrane interactions lead to Aβ_{42} folding. The differences between the two systems further manifest themselves in the structural preferencs of Aβ_{42}. The evolution of the secondary structure per residue (Fig. S5) reveals a preference for β-sheet formation for the individual Aβ_{42} peptide interacting with the membrane, while in addition to β-sheets also helices form when a POPC lipid is bound to the membrane-interacting Aβ_{42} peptide. This reinforces the observation from the 1:3 complex simulations that lipid binding to Aβ_{42} can cause a coil-to-helix transition. However, the helical structure encountered in the membrane simulation is different from the helix-kink-helix structure described above. Here, the highest helical propensity resulted between residues Phe20 and Met35, which include the region with the deepest insertion into the membrane. This again suggests that membrane insertion of Aβ_{42} is likely to take place via a helical structure; a possible beginning of this process might be presented by the snapshot shown in Fig. 5a (bottom). Without the extra POPC lipid, very few helices formed in the simulations (Fig. S5). Instead, an increased amount of β-sheets were found compared to the individual peptide or when in complex with a single POPC lipid (Fig. S2). However, the β-sheet structures did not insert into the membrane, but rather adsorbed to its surface, as can be seen in the representative snapshot in Fig. 5a (top).

In order to confirm our observation that helix formation and Aβ_{42}–membrane interactions are indeed correlated, we calculated the helical content and plotted this quantity against the number of contacts that formed between Aβ_{42} and the membrane (Fig. 5d). In both systems the amount of helix increases with increasing Aβ_{42}–membrane contacts. This effect is more pronounced for the Aβ_{42}–POPC complex, where helix formation is already observed when only few contacts between the peptide and the membrane are present. This suggests that the helix formation is a cooperative effect exerted by the single lipid and the membrane on Aβ_{42}. This bears similarities with the effects that the three lipids can have on the peptide in a 1:3 complex; however, the amount of helix observed here does not reach beyond 20%, while in run 1 of the 1:3 complex simulations, ≈45% of the residues adopted a helical state.

In summary, while no deep membrane insertion of Aβ_{42} was observed here, our results provide evidence on the possible membrane insertion mechanism of the Aβ_{42} peptide, which is likely to proceed via a helical structure and is assisted by bound lipids.

4. Discussion and conclusion

Our simulations revealed the formation of stable complexes between Aβ_{42} and lipids in 1:1 and 1:3 ra-

tios. This observation is in good agreement with the MD studies by La Rosa and coworkers [35, 34] who also reported the formation of stable protein–lipid complexes for Aβ_{40}, Aβ_{42}, human and rat amylin. Our findings highlight that Aβ_{42} remains largely disordered when in complex with only one POPC or DPPC lipid, whereas the binding of three lipid molecules triggers a disorder-order transition upon which the peptide folds into either a helical or β-sheet structure. This observation partly agrees with the findings by La Rosa *et al.* who reported an increase in helical content upon Aβ–lipid complex formation. A an α-helical content of 45% developed in one of our triplicate simulations of the 1:3 Aβ42–POPC complexes. It is a helix-kink-helix structure, which is stabilized by hydrophobic interactions between the lipid tails and the hydrophobic residues Leu17, Ala21, Ile32, and Val36. Similar Aβ structures have also been predicted from NMR experiments of the micelle-bound peptide [53, 54, 55, 56, 57]. In fact, in our simulations this helical structure is only stable when the mentioned residues were simultaneously in contact with the lipids. This lets us conclude that Aβ's hydrophobicity is not sufficient for its folding by itself, but it can do so following its binding to a hydrophobic interaction partner. This is a typical behavior of IDPs where conformation switching can be induced by binding of an IDP to an interaction partner [13]. Another characteristic of IDPs is that the resulting structure following binding can vary depending on the interaction partner [58]. Such binding plasticity is also found here for Aβ_{42}, as it can as well fold into a β-sheet following its binding to three POPC lipids.

The complex stability in solution encouraged us to address its likelihood to drive insertion of Aβ_{42} into a lipid membrane, especially when considering our observation of a single POPC lipid inserting into a POPC membrane within a microsecond of simulation, where the insertion event itself was completed within 10 ns. However, within 2 μs of our all-atom MD simulations, the peptide did not fully insert into the POPC membrane, neither when simulated as individual peptide, nor when in complex with a POPC lipid. Nonetheless, the presence of a POPC lipid bound to Aβ_{42} did have some effects on the membrane-bound Aβ_{42}. First, it encouraged the formation of a helical structure, whereas without the lipid random coil and β-sheets were the dominating structures. Second, the helical structure in complex with a lipid was able to dip deeper into the membrane than the peptide alone. Despite the absence of full membrane insertion in our simulations, these observations indicate, as suggested by the lipid-chaperone hypothesis [35, 34], that Aβ_{42}–lipid complex formation decreases the energy barrier for membrane insertion. Moreover, it encourages Aβ_{42} to fold into a helical structure that seems to be needed for membrane insertion [53, 54, 55, 56, 57, 59].

For the membrane-bound Aβ_{42} we recorded β-sheet formation when not in complex with an additional lipid. This finding contrasts to our recent study of Aβ_{42} dimerization at a neuronal membrane [60]. While we observed a random coil to β-sheet transition upon dimerization that seems on pathway to amyloid aggregation in solution, the interactions with the neuronal membrane decreased the order of the Aβ_{42} dimer by attenuating its propensity to form a β-sheet structure. This results from the interactions of Aβ_{42} with the surface-exposed sugar groups of the gangliosides GM1, which turned out to be the main interaction partners of Aβ_{42}. This shows that in our future studies testing the lipid-chaperone hypothesis, we should and will include more realistic cell models. Moreover, we will also study the effects of Aβ_{42}–lipid complexes with higher lipid ratios, as the current results of the 1:3 complexes already indicate that under these circumstances the lipids have a more pronounced effect. Finally, while our simulations are already on the microsecond timescale, future simulations on the same subject should be even longer, lasting for tens of microseconds, and the application of enhanced sampling methods should be considered too [61, 62].

Conflict of interest

None declared.

Acknowledgments

H.F. and B.S. acknowledge funding for this project from the Palestinian-German Science Bridge financed by the German Federal Ministry of Education and Research. J.L. and B.S. received funding for this project from the Deutsche Forschungsgemeinschaft (German Research Foundation, https://www.dfg.de/) through Grant 267205415 (CRC 1208, Project A07). Computational infrastructure and support for performing the MD simulations were provided by the Centre for Information and Media Technology at Heinrich Heine University Düsseldorf.

References

[1] A. K. Dunker, J. D. Lawson, C. J. Brown, R. M. Williams, P. Romero, J. S. Oh, C. J. Oldfield, A. M. Campen, C. M. Ratliff, K. W. Hipps, et al., Intrinsically disordered protein, Journal of molecular graphics and modelling 19 (1) (2001) 26–59.

[2] D. Eliezer, Biophysical characterization of intrinsically disordered proteins, Current opinion in structural biology 19 (1) (2009) 23–30.

[3] M.-K. Yoon, D. M. Mitrea, L. Ou, R. W. Kriwacki, Cell cycle regulation by the intrinsically disordered proteins p21 and p27, Biochemical Society Transactions 40 (5) (2012) 981–988.

[4] A. S. Garza, N. Ahmad, R. Kumar, Role of intrinsically disordered protein regions/domains in transcriptional regulation, Life sciences 84 (7-8) (2009) 189–193.

[5] A. Bah, R. M. Vernon, Z. Siddiqui, M. Krzeminski, R. Muhandiram, C. Zhao, N. Sonenberg, L. E. Kay, J. D. Forman-Kay, Folding of an intrinsically disordered protein by phosphorylation as a regulatory switch, Nature 519 (7541) (2015) 106–109.

[6] H. J. Dyson, P. E. Wright, Intrinsically unstructured proteins and their functions, Nature reviews Molecular cell biology 6 (3) (2005) 197–208.

[7] K. Rajagopalan, R. Qiu, S. M. Mooney, S. Rao, T. Shiraishi, E. Sacho, H. Huang, E. Shapiro, K. R. Weninger, P. Kulkarni, The stress-response protein prostate-associated gene 4, interacts with c-jun and potentiates its transactivation, Biochim. Biophys. Acta Mol. Basis Dis. 1842 (2) (2014) 154–163.

[8] P. Kulkarni, M. K. Jolly, D. Jia, S. M. Mooney, A. Bhargava, L. T. Kagohara, Y. Chen, P. Hao, Y. He, R. W. Veltri, et al., Phosphorylation-induced conformational dynamics in an intrinsically disordered protein and potential role in phenotypic heterogeneity, Proc. Natl. Acad. Sci. U.S.A. 114 (13) (2017) E2644–E2653.

[9] X. Lin, P. Kulkarni, F. Bocci, N. P. Schafer, S. Roy, M.-Y. Tsai, Y. He, Y. Chen, K. Rajagopalan, S. M. Mooney, et al., Structural and dynamical order of a disordered protein: Molecular insights into conformational switching of page4 at the systems level, Biomolecules 9 (2) (2019) 77–95.

[10] D. Parker, K. Ferreri, T. Nakajima, V. LaMorte, R. Evans, S. Koerber, C. Hoeger, M. Montminy, Phosphorylation of creb at ser-133 induces complex formation with creb-binding protein via a direct mechanism., Mol. Cell. Biol. 16 (2) (1996) 694–703.

[11] D. Parker, M. Rivera, T. Zor, A. Henrion-Caude, I. Radhakrishnan, A. Kumar, L. H. Shapiro, P. E. Wright, M. Montminy, P. K. Brindle, Role of secondary structure in discrimination between constitutive and inducible activators, Mol. Cell. Biol. 19 (8) (1999) 5601–5607.

[12] H. Liu, X. Guo, J. Han, R. Luo, H.-F. Chen, Order-disorder transition of intrinsically disordered kinase inducible transactivation domain of creb, J. Chem. Phys. 148 (22) (2018) 225101.

[13] B. Strodel, Energy landscapes of protein aggregation and conformation switching in intrinsically disordered proteins, J. Mol. Biol. (2021) 167182doi:https://doi.org/10.1016/j.jmb.2021.167182.

[14] P. Kulkarni, V. N. Uversky, Intrinsically disordered proteins in chronic diseases (2019).

[15] V. N. Uversky, Amyloidogenesis of natively unfolded proteins, Current Alzheimer Research 5 (3) (2008) 260–287.

[16] Z. Du, V. N. Uversky, A comprehensive survey of the roles of highly disordered proteins in type 2 diabetes, International journal of molecular sciences 18 (10) (2017) 2010.

[17] V. N. Uversky, The triple power of d (3): protein intrinsic disorder in degenerative diseases, Front Biosci (Landmark Ed) 19 (2014) 181–258.

[18] V. N. Uversky, Intrinsic disorder in proteins associated with neurodegenerative diseases, Protein folding and misfolding: neurodegenerative diseases (2009) 21–75.

[19] F. Chiti, C. M. Dobson, Protein misfolding, functional amyloid, and human disease, Annu. Rev. Biochem. 75 (2006) 333–366.

[20] M. Querol-Vilaseca, M. Colom-Cadena, J. Pegueroles, R. Nuñez-Llaves, J. Luque-Cabecerans, L. Muñoz-Llahuna, J. Andilla, O. Belbin, T. L. Spires-Jones, E. Gelpi, et al., Nanoscale structure of amyloid-β plaques in alzheimer's disease, Scientific reports 9 (1) (2019) 1–10.

[21] G. K. Gouras, C. G. Almeida, R. H. Takahashi, Intraneuronal aβ accumulation and origin of plaques in alzheimer's disease, Neurobiology of aging 26 (9) (2005) 1235–1244.

[22] S. Sadigh-Eteghad, B. Sabermarouf, A. Majdi, M. Talebi, M. Farhoudi, J. Mahmoudi, Amyloid-beta: a crucial factor in alzheimer's disease, Medical principles and practice 24 (1) (2015) 1–10.

[23] P. H. Reddy, M. F. Beal, Amyloid beta, mitochondrial dysfunction and synaptic damage: implications for cognitive decline in aging and alzheimer's disease, Trends in molecular medicine 14 (2) (2008) 45–53.

[24] S. J. C. Lee, E. Nam, H. J. Lee, M. G. Savelieff, M. H. Lim, Towards an understanding of amyloid-β oligomers: characterization, toxicity mechanisms, and inhibitors, Chemical Society Reviews 46 (2) (2017) 310–323.

[25] M. C. Owen, D. Gnutt, M. Gao, S. K. Wärmländer, J. Jarvet, A. Gräslund, R. Winter, S. Ebbinghaus, B. Strodel, Effects of in vivo conditions on amyloid aggregation, Chemical Society Reviews 48 (14) (2019) 3946–3996.

[26] C. A. McLean, R. A. Cherny, F. W. Fraser, S. J. Fuller, M. J. Smith, K. Vbeyreuther, A. I. Bush, C. L. Masters, Soluble pool of aβ amyloid as a determinant of severity of neurodegeneration in alzheimer's disease, Annals of neurology 46 (6) (1999) 860–866.

[27] M. D. Kirkitadze, G. Bitan, D. B. Teplow, Paradigm shifts in alzheimer's disease and other neurodegenerative disorders: the emerging role of oligomeric assemblies, Journal of neuroscience research 69 (5) (2002) 567–577.

[28] K. Broersen, F. Rousseau, J. Schymkowitz, The culprit behind amyloid beta peptide related neurotoxicity in alzheimer's disease: oligomer size or conformation?, Alzheimer's research & therapy 2 (4) (2010) 1–14.

[29] A. D. Korczyn, The amyloid cascade hypothesis, Alzheimer's & dementia 4 (3) (2008) 176–178.

[30] C. Reitz, Alzheimer's disease and the amyloid cascade hypothesis: a critical review, International journal of Alzheimer's disease 2012.

[31] E. N. Cline, M. A. Bicca, K. L. Viola, W. L. Klein, The amyloid-β oligomer hypothesis: beginning of the third decade, Journal of Alzheimer's Disease 64 (s1) (2018) S567–S610.

[32] F. Scollo, C. Tempra, F. Lolicato, M. F. Sciacca, A. Raudino, D. Milardi, C. La Rosa, Phospholipids critical micellar concentrations trigger different mechanisms of intrinsically disordered proteins interaction with model membranes, The journal of physical chemistry letters 9 (17) (2018) 5125–5129.

[33] F. Scollo, C. La Rosa, Amyloidogenic intrinsically disordered proteins: New insights into their self-assembly and their interaction with membranes, Life 10 (8) (2020) 144.

[34] M. F. Sciacca, F. Lolicato, C. Tempra, F. Scollo, B. R. Sahoo, M. D. Watson, S. García-Viñuales, D. Milardi, A. Raudino, J. C. Lee, et al., Lipid-chaperone hypothesis: A common molecular mechanism of membrane disruption by intrinsically disordered proteins, ACS chemical neuroscience.

[35] C. La Rosa, S. Scalisi, F. Lolicato, M. Pannuzzo, A. Raudino, Lipid-assisted protein transport: A diffusion-reaction model supported by kinetic experiments and molecular dynamics simulations, The Journal of chemical physics 144 (18) (2016) 184901.

[36] M. B. Rone, J. Fan, V. Papadopoulos, Cholesterol transport in steroid biosynthesis: role of protein–protein interactions and implications in disease states, Biochimica et Biophysica Acta (BBA)-Molecular and Cell Biology of Lipids 1791 (7) (2009)

646–658.

[37] J. Sandhu, S. Li, L. Fairall, S. G. Pfisterer, J. E. Gurnett, X. Xiao, T. A. Weston, D. Vashi, A. Ferrari, J. L. Orozco, et al., Aster proteins facilitate nonvesicular plasma membrane to er cholesterol transport in mammalian cells, Cell 175 (2) (2018) 514–529.

[38] M. S. Abreu, L. M. Estronca, M. J. Moreno, W. L. Vaz, Binding of a fluorescent lipid amphiphile to albumin and its transfer to lipid bilayer membranes, Biophysical journal 84 (1) (2003) 386–399.

[39] L. Martínez, R. Andrade, E. G. Birgin, J. M. Martínez, Packmol: A package for building initial configurations for molecular dynamics simulations, Journal of Computational Chemistry 30 (13) (2009) 2157–2164. doi:https://doi.org/10.1002/jcc.21224.

[40] P. Robustelli, S. Piana, D. Shaw, Developing a molecular dynamics force field for both folded and disordered protein states, Proc. Natl. Acad. Sci. U.S.A. 115 (2018) 201800690. doi:10.1073/pnas.1800690115.

[41] A. Paul, S. Samantray, M. Anteghini, B. Strodel, Thermodynamics and kinetics of the amyloid-β peptide revealed by markov state models based on md data in agreement with experiment, Chem. Sci. 12 (2021) 6652–6669. doi:10.1039/D0SC04657D.

[42] J. Lee, X. Cheng, J. M. Swails, M. S. Yeom, P. K. Eastman, J. A. Lemkul, S. Wei, J. Buckner, J. C. Jeong, Y. Qi, et al., Charmm-gui input generator for namd, gromacs, amber, openmm, and charmm/openmm simulations using the charmm36 additive force field, Journal of chemical theory and computation 12 (1) (2016) 405–413.

[43] M. J. Abraham, T. Murtola, R. Schulz, S. Páll, J. C. Smith, B. Hess, E. Lindahl, Gromacs: High performance molecular simulations through multi-level parallelism from laptops to supercomputers, SoftwareX 1 (2015) 19–25.

[44] J. Huang, S. Rauscher, G. Nawrocki, R. Ting, M. Feig, B. de Groot, H. Grubmüller, A. MacKerell, Charmm36m: An improved force field for folded and intrinsically disordered proteins, Nature Meth. 14 (2017) 71–73. doi:10.1038/nmeth.4067.

[45] S. Samantray, F. Yin, B. Kav, B. Strodel, Different force fields give rise to different amyloid aggregation pathways in molecular dynamics simulations, J. Chem. Inf. Model. 60 (12) (2021) 6462 – 6475.

[46] R. W. Pastor, A. D. MacKerell, Development of the charmm force field for lipids, J. Phys. Chem. Lett. 2 (13) (2011) 1526–1532. doi:10.1021/jz200167q.

[47] W. L. Jorgensen, J. Chandrasekhar, J. D. Madura, R. W. Impey, M. L. Klein, Comparison of simple potential functions for simulating liquid water, J. Chem. Phys. 79 (2) (1983) 926–935. doi:10.1063/1.445869.

[48] P. Mark, L. Nilsson, Structure and dynamics of the TIP3P, SPC, and SPC/E water models at 298 K, J. Phys. Chem. A 105 (43) (2001) 9954–9960. doi:10.1021/jp003020w.

[49] G. Bussi, D. Donadio, M. Parrinello, Canonical sampling through velocity rescaling, The Journal of chemical physics 126 (1) (2007) 014101.

[50] H. J. Berendsen, J. v. Postma, W. F. van Gunsteren, A. DiNola, J. R. Haak, Molecular dynamics with coupling to an external bath, The Journal of chemical physics 81 (8) (1984) 3684–3690.

[51] T. Darden, D. York, L. Pedersen, Particle mesh Ewald: An N·log(N) method for Ewald sums in large systems, J. Chem. Phys.doi:10.1063/1.464397.

[52] W. Kabsch, C. Sander, Dictionary of protein secondary structure: Pattern recognition of hydrogen-bonded and geometrical features, Biopolymers 22 (12) (1983) 2577–2637. doi:10.1002/bip.360221211.

[53] M. Coles, W. Bicknell, A. A. Watson, D. P. Fairlie, D. J. Craik, Solution structure of amyloid β-peptide(1–40) in a water–micelle environment. is the membrane-spanning domain where we think it is?, Biochemistry 37 (1998) 11064–11077.

[54] H. Shao, S. Jao, K. Ma, M. G. Zagorski, Solution structures of micelle-bound amyloid beta-(1-40) and beta-(1-42) peptides of alzheimer's disease, J. Mol. Biol. 285 (1999) 755–773.

[55] J. Jarvet, J. Danielsson, P. Damberg, M. Oleszczuk, A. Gräslund, Positioning of the alzheimer abeta(1-40) peptide in sds micelles using nmr and paramagnetic probes., J. Biomol. NMR 39 (2007) 63–72.

[56] O. Crescenzi, S. Tomaselli, R. Guerrini, S. Salvadori, A. M. D'Ursi, P. A. Temussi, D. Picone, Solution structure of the alzheimer amyloid β-peptide (1-42) in an apolar microenvironment., Eur. J. Biochem. 269 (2002) 5642–5648.

[57] H. Sticht, P. Bayer, D. Willbold, S. Dames, C. Hilbich, K. Beyreuther, R. W. Frank, P. Rösch, Structure of amyloid a4-(1-40)-peptide of alzheimer's disease, Eur. J. Biochem. 233 (1995) 293–298.

[58] V. N. Uversky, A decade and a half of protein intrinsic disorder: biology still waits for physics, Protein Sci. 22 (6) (2013) 693–724.

[59] N. Miyashita, J. E. Straub, D. Thirumalai, Structures of β-amyloid peptide 1–40, 1–42, and 1–55—the 672–726 fragment of app—in a membrane environment with implications for interactions with γ-secretase, J. Am. Chem. Soc. 131 (2009) 17843–17852.

[60] H. Fatafta, M. Khaled, M. C. Owen, A. Sayyed-Ahmad, B. Strodel, Amyloid-β peptide dimers undergo a random coil to β-sheet transition in the aqueous phase but not at the neuronal membrane, Proc. Natl. Acad. Sci. USA 118 (2021) e2106210118. doi:10.1073/pnas.2106210118.

[61] M. Carballo-Pacheco, B. Strodel, Advances in the simulation of protein aggregation at the atomistic scale, J. Phys. Chem. B 120 (2016) 2991–2999. doi:10.1021/acs.jpcb.6b00059.

[62] B. Strodel, Amyloid aggregation simulations: challenges, advances and perspectives, Curr. Opin. Struct. Biol. 67 (2021) 145–152. doi:10.1016/j.sbi.2020.10.019.